

See discussions, stats, and author profiles for this publication at: <https://www.researchgate.net/publication/264247269>

# Distance and Plasmon Wavelength Dependent Fluorescence of Molecules Bound to Silica-Coated Gold Nanorods

ARTICLE in ACS NANO · JULY 2014

Impact Factor: 12.88 · DOI: 10.1021/nn502887j · Source: PubMed

---

CITATIONS

26

---

READS

195

## 4 AUTHORS, INCLUDING:



William Larry Wilson

Harvard University

84 PUBLICATIONS 3,609 CITATIONS

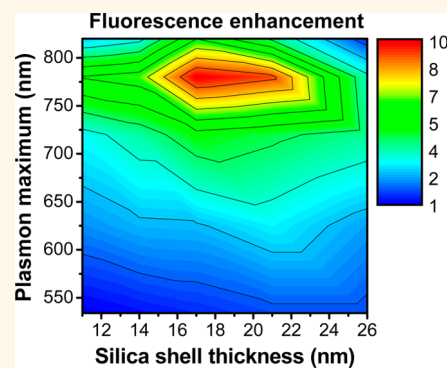
SEE PROFILE

# Distance and Plasmon Wavelength Dependent Fluorescence of Molecules Bound to Silica-Coated Gold Nanorods

Nardine S. Abadeer,<sup>†</sup> Marshall R. Brennan,<sup>†</sup> William L. Wilson,<sup>‡</sup> and Catherine J. Murphy<sup>†,\*</sup>

<sup>†</sup>Department of Chemistry and <sup>‡</sup>Department of Materials Science and Engineering, Frederick Seitz Materials Research Laboratory, University of Illinois at Urbana—Champaign, Urbana, Illinois 61801, United States

**ABSTRACT** Plasmonic nanoparticles can strongly interact with adjacent fluorophores, resulting in plasmon-enhanced fluorescence or fluorescence quenching. This dipolar coupling is dependent upon nanoparticle composition, distance between the fluorophore and the plasmonic surface, the transition dipole orientation, and the degree of spectral overlap between the fluorophore's absorbance/emission and the surface plasmon band of the nanoparticles. In this work, we examine the distance and plasmon wavelength dependent fluorescence of an infrared dye ("IRDye") bound to silica-coated gold nanorods. Nanorods with plasmon band maxima ranging from 530 to 850 nm are synthesized and then coated with mesoporous silica shells 11–26 nm thick. IRDye is covalently attached to the nanoparticle surface *via* a click reaction. Steady-state fluorescence measurements demonstrate plasmon wavelength and silica shell thickness dependent fluorescence emission. Maximum fluorescence intensity, with approximately 10-fold enhancement, is observed with 17 nm shells when the nanorod plasmon maximum is resonant with IRDye absorption. Time-resolved photoluminescence reveals multiexponential decay and a sharp reduction in fluorescence lifetime with decreasing silica shell thickness and when the plasmon maximum is closer to IRDye absorption/emission. Control experiments are carried out to confirm that the observed changes in fluorescence are due to plasmonic interactions, is simply surface attachment. There is no change in fluorescence intensity or lifetime when IRDye is bound to mesoporous silica nanoparticles. In addition, IRDye loading is limited to maintain a distance between dye molecules on the surface to more than 9 nm, well above the Förster radius. This assures minimal dye–dye interactions on the surface of the nanoparticles.



**KEYWORDS:** plasmon-enhanced fluorescence · gold nanorods · IRDye · fluorescence lifetime · dye–nanoparticle interactions

Gold nanorods are rod-shaped plasmonic nanoparticles with tunable, size dependent optical responses and a wide array of unique optical properties.<sup>1–3</sup> The collective oscillation of conduction band electrons on the surface of gold nanorods gives rise to two plasmonic resonance bands, the wavelengths of which are defined by nanorod aspect ratio and can be tuned from the visible to the near-infrared.<sup>4–6</sup> Gold nanorods strongly absorb and scatter light, especially at wavelengths resonant with their surface plasmons. Due to photon confinement, strong electromagnetic fields are generated at the metal surface.<sup>4,7</sup> Electromagnetic field effects give rise to a variety of optical processes such as laser photothermal heating,<sup>8</sup> Raman resonances,<sup>9</sup> two-photon absorption,<sup>10</sup> and emission<sup>11–15</sup> which are often enhanced near a gold nanorod surface.

It is known that fluorescence excitation and emission processes can be altered when a fluorophore is near a plasmonic nanoparticle.<sup>16,17</sup> The electromagnetic field strength is most concentrated at the surface of plasmonic nanoparticles and decays exponentially as a function of distance. The nanoparticle and fluorophore form an electromagnetically coupled system, which when excited leads to additional de-excitation pathways. This results in higher excitation rates and/or enhanced radiative decay rates of the fluorophore and fluorescence emission enhancement.<sup>11–13</sup> However, in some instances, fluorescence may instead be quenched if the excited fluorophores relax rapidly by nonradiative energy transfer into the surface plasmon resonance.<sup>18,19</sup>

Because of these two competing processes, literature values of enhancement are

\* Address correspondence to murphycj@illinois.edu.

Received for review May 27, 2014 and accepted July 25, 2014.

Published online July 25, 2014  
10.1021/nn502887j

© 2014 American Chemical Society

strongly varied. Researchers have observed nearly 100% emission quenching to over 1000-fold enhancement in emission intensity.<sup>11–25</sup> Of course, both enhancement and quenching of fluorescence are distance dependent. At a certain distance from the plasmonic surface, energy transfer into the plasmon is reduced but the electromagnetic field strength can still be great enough to enhance fluorescence emission.<sup>15,16</sup> Strong enhancement has been observed in the 10–20 nm range from the plasmonic surface.<sup>20–23</sup> In addition, fluorescence near plasmonic nanoparticles is dependent on plasmon maximum. Some researchers have suggested that fluorescence coupling to the nanoparticle may be stronger when the plasmon band overlaps with a fluorophore's absorbance or emission profile. Since gold nanorod plasmon bands are easily tuned from 500 to over 900 nm, gold nanorods are useful for studies of plasmon-enhanced fluorescence with a wide range of fluorophores.<sup>15,24,25</sup>

If applications of plasmon-enhanced fluorescence techniques are to be realized, it is essential to gain more insight into the phenomenon of plasmon-enhanced fluorescence. Fluorescent molecules are used in imaging and sensing studies with biological and electronic applications ranging from detection of biomarkers of disease to single-molecule imaging and organic electronics. However, fluorophores are often unstable, with low quantum yields and can be highly sensitive to photobleaching. This is especially true for near-infrared fluorophores, limiting their potential applications.<sup>11,15,16,26</sup> Enhancement of fluorescence emission *via* coupling to plasmonic particles is one potential method to increase the effectiveness of weak fluorophores.<sup>14,15</sup>

To date, fluorescence enhancement studies have mainly focused on gold or silver nanostructured surfaces or nanoparticles immobilized on a surface.<sup>16,25</sup> This allows for good control of nanoparticle–fluorophore distance, and nanoparticle aggregation is reduced; however, applications of fluorescence enhancement in this geometry are rather limited.<sup>27</sup> There are some examples of fluorescence enhancement with colloidal nanomaterials, but control of fluorophore–particle distance is more difficult to achieve. Often times, the fluorophore is incorporated into a shell or between polymer layers *versus* on the surface.<sup>11–24</sup> In addition, dye–surface and dye–dye interactions are rarely accounted for when trying to understand changes in fluorescence behavior.<sup>21</sup> To our knowledge, there are no solution-based studies, with gold nanorods, that include both distance and plasmon wavelength dependent fluorescence. Moreover, none explore and exclude possible dye–dye interactions or dye–surface interactions that may impact fluorescence behavior near gold nanorods.

In order to gain a deeper understanding of plasmon-enhanced fluorescence, we carried out a study of

distance and plasmon wavelength dependent fluorescence of an infrared dye (“IRDye”) bound to silica-coated gold nanorods. IRDye 800CW DBCO has a dibenzylcyclooctyne (DBCO) functionality allowing for attachment to azides *via* click chemistry. The IRDye imaging agents, developed by LI-COR, are specially designed to potentially aid in disease detection and to monitor drug treatments.<sup>28</sup> IRDye absorbance/emission profiles are in the “water window” (700–1100 nm), so they are potentially useful in biological applications. However, IRDye has a quantum yield of only 0.07, limiting its application. Therefore, it could serve as a good candidate for plasmon-enhanced fluorescence.<sup>11</sup> Gold nanorods are ideal for studies of plasmon-enhanced fluorescence. Gold does not experience oxidation that often occurs with silver, and gold nanorods absorb/scatter more strongly than smaller gold spheres, resulting in stronger field effects. In addition, gold nanorod plasmon bands are readily tuned by changing the aspect ratio; this enables the wavelength dependence of fluorescence to be easily studied.<sup>4,15,21</sup>

To this end, gold nanorods of varying aspect ratio having plasmon maxima ranging from 530 to 850 nm are prepared. At 530 nm, there is no spectral overlap with IRDye 800CW DBCO which absorbs/emits at 779/794 nm, but there is stronger overlap with higher aspect ratios. A dielectric spacer is used to achieve distance dependence. The gold nanorods are coated in 11–26 nm thick mesoporous silica *via* modification of the Stöber method.<sup>29,30</sup> 3-Azidopropyltrimethoxysilane is synthesized and used to functionalize the silica surface. IRDye is then conjugated to the azide-functionalized surface *via* a copper-free click reaction, and the amount of IRDye attached to the surface of the nanorods is quantified. Fluorescence of IRDye–nanorod conjugates is monitored using steady-state and time-resolved measurements to determine changes in fluorescence intensity and fluorescence lifetime. Control experiments of IRDye bound to silica nanoparticles are carried out to confirm that changes in fluorescence are due to plasmonic interactions, not attachment of the fluorophore to a silica surface. In addition, an experiment varying the number of dye molecules per particle is carried out to assess how separation between dye molecules on the surface of the nanoparticles may affect fluorescence emission. Based on this result, IRDye loading is limited to prevent dye–dye quenching.

## RESULTS AND DISCUSSION

**Nanoparticle Design.** IRDye was chosen for this study because of its potential biological application, low quantum yield, and absorbance/emission profile. The molecular structure of IRDye 800CW DBCO (Figure 1a) contains a DBCO tether.<sup>28</sup> The DBCO group allows for conjugation to azides *via* 1,3-dipolar cycloaddition generating a 1,2,3-triazole. Traditionally, click chemistry with azides and terminal alkynes is carried out

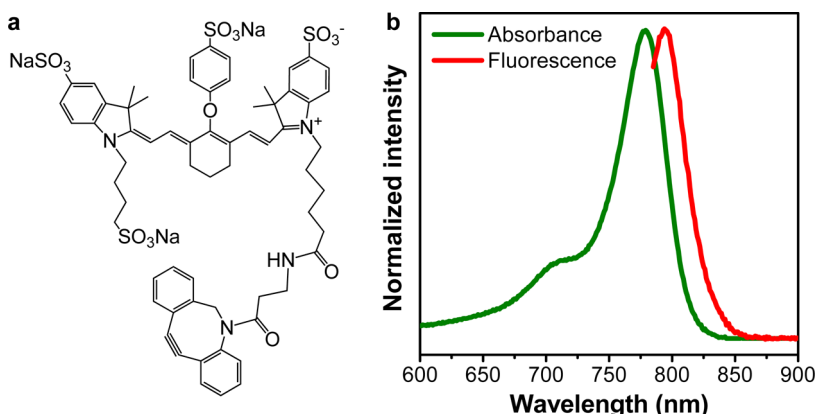


**Figure 1.** (a) Structure of IRDye 800CW DBCO. (b) IRDye absorbance and emission in MeOH with maximum absorbance/emission at 779/794 nm.

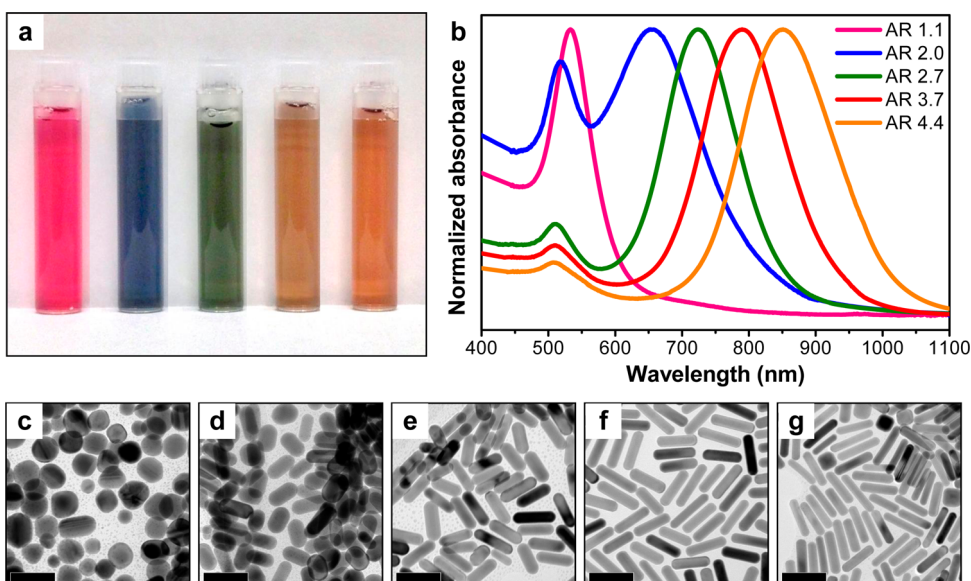
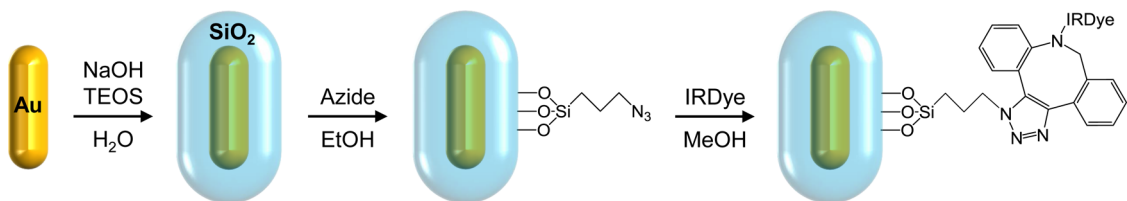


**Figure 2.** (a) Photograph of gold nanorod solutions with increasing aspect ratio left to right. (b) UV–vis absorbance spectra of gold nanorods with different aspect ratios. TEM images of gold nanorods (c) AR 1.1, (d) AR 2.0, (e) AR 2.7, (f) AR 3.7, and (g) AR 4.4. Scale bars = 50 nm.

using a copper catalyst.<sup>31</sup> However, azides can also react with internal alkynes in a strain-promoted reaction. This eliminates the need for copper, which is cytotoxic, and the click reaction can proceed quickly at room temperature in a range of solvents.<sup>32</sup> The absorbance and fluorescence emission spectra of IRDye in methanol (Figure 1b) indicate maximum absorbance/emission at 779/794 nm. The quantum yield of IRDye 800CW DBCO in methanol (MeOH) is  $0.075 \pm 0.005$  (Supporting Information Table S1). The obtained value is close to a previous calculation of IRDye in water.<sup>11</sup> Because IRDye has such a low quantum yield, it is an ideal candidate for studies of plasmon-enhanced fluorescence.

A library of cetyltrimethylammonium bromide (CTAB)-coated gold nanorods of varying aspect ratio was prepared using our well-known seed-mediated growth procedure.<sup>33</sup> Gold seeds were added to a growth solution containing CTAB, HAuCl<sub>4</sub>·3H<sub>2</sub>O, AgNO<sub>3</sub>,

and ascorbic acid. A CTAB bilayer on the surface of gold nanorods helps to prevent nanorod aggregation, and the addition of AgNO<sub>3</sub> to the growth solution facilitates anisotropic growth, allowing for control of aspect ratio (AR).<sup>2</sup> This allows for variation in longitudinal plasmon maxima and therefore variation in spectral overlap between gold nanorods and IRDye. Five aspect ratios of CTAB-coated gold nanorods were prepared and purified (Figure 2a). UV–vis absorbance spectra of the CTAB-coated gold nanorods in water show plasmon band maxima located at 533, 653, 724, 790, and 851 nm (Figure 2b). These wavelengths correspond to AR 1.1, AR 2.0, AR 2.7, AR 3.7, and AR 4.4 nanorods, respectively. These aspect ratios of nanorods were selected because the plasmon bands ranged from almost no overlap to strong spectral overlap with IRDye absorbance/emission. Transmission electron microscopy (TEM) images are shown in Figure 2c–g and were used to calculate aspect ratio. The absolute dimensions, plasmon maxima, and



**Scheme 1.** Attachment of IRDye to gold nanorods. Gold nanorods were coated in silica and then functionalized with 3-azidopropyltrimethoxysilane. IRDye molecules were linked to the azide-functionalized surface *via* copper-free, azide–alkyne cycloaddition.

calculated aspect ratios of the CTAB gold nanorods are listed in Table S2.

Attachment of IRDye and variation of dye–metal distance was achieved through silica coating and then silane functionalization of the CTAB-coated gold nanorods (Scheme 1). A dielectric spacer, like silica, allows for good control of dye–metal distance, and it is easy to measure thickness by TEM. In addition, a silica coating reduces nanorod aggregation, increases solubility of gold nanorods in organic solvents, and is easy to functionalize with various silanes.<sup>29</sup> Silica is known to modify the electromagnetic field around plasmonic nanoparticles, but the effect on electromagnetic field strength is minimal past 10 nm when there is a complete silica shell.<sup>34,35</sup> Silica-coated gold nanorods were functionalized with an azide linker to facilitate IRDye attachment to surface. Since azide–alkyne click reactions are highly specific, unwanted side reactions within the IRDye molecule were prevented with this attachment method.<sup>32</sup> Potential dye–dye interactions on the silica surfaces were also avoided by limiting IRDye loading. This allowed us to accurately determine distance and plasmon wavelength dependent fluorescence behavior.

Silica coating was carried out through modification of the well-known Stöber process.<sup>30</sup> The hydrolysis and condensation of tetralkylsilicates to form silica can be catalyzed by a change in pH. Previous researchers have demonstrated 15 nm coatings of mesoporous silica around CTAB-coated metal nanoparticles, including gold nanorods.<sup>29</sup> CTAB micelles are a template for silica deposition through the hydrolysis and condensation of the silica precursor tetraethylorthosilicate (TEOS). Growth of mesoporous silica on the nanoparticle surface is attributed to a three-stage mechanism: silica oligomerization, formation of silica/CTAB particles, and aggregation of these silica/CTAB particles.<sup>36</sup> Since CTAB is mostly surrounding the nanorods, the silica/CTAB particles form and aggregate on the nanorod surface, limiting formation of free silica nanoparticles.<sup>29,36</sup>

Through careful control of reaction parameters, we were able to achieve highly reproducible and robust silica coatings. Five silica shell thicknesses ranging from 11 to 26 nm were coated on each of the five aspect ratios of gold nanorods used. Previous researchers have demonstrated that reaction time or TEOS concentration can be used to control silica thickness on

gold nanorods. However, we found that these procedures were difficult to reproduce batch-to-batch and 2–5 nm increments in shell thickness were difficult to achieve.<sup>29,37</sup> Instead, we demonstrate here that the most critical component to control silica coating of gold nanorods is CTAB concentration. As-synthesized gold nanorods are prepared in 0.1 M CTAB, which is far above the critical micelle concentration of 1 mM in pure water.<sup>38</sup> In order to control CTAB concentration, gold nanorods were centrifuged twice after synthesis, so the concentration of CTAB was less than 0.01 mM. Additional centrifugation steps were not carried out because complete CTAB removal from the surface causes gold nanorod aggregation. Then, different amounts CTAB were added to the gold nanorod solutions, and the solutions were mixed to allow the CTAB to equilibrate on the surface. Silica coating was carried out by first adjusting the pH using NaOH, then adding TEOS and mixing the solutions for several hours. In the silica coating reactions, concentration of CTAB was varied between 1.2 and 0.4 mM to obtain porous shells about 11, 14, 17, 22, and 26 nm thick (Figure 3).

The amount of CTAB free in solution is critical to silica shell thickness. As the CTAB concentration increases, more CTAB is free in solution *versus* on the nanorod surface and silica shell thickness decreases (Figure 4a). When the concentration is well past the critical micelle concentration of CTAB, around 2 mM, no silica is formed on the nanorod surface. Fortunately, most silica formed apart from the nanorods is removed by centrifugation after the coating reaction. In addition to CTAB concentration, gold nanorod concentration, pH, TEOS concentration, reaction temperature, and reaction time were all tightly controlled. The concentration of each batch of gold nanorods used during silica coating was kept high, further limiting excess silica particle formation. We also found that adjusting the pH to 10 is optimal. At higher pH values, the silica shells are of poor quality and no silica forms below pH 9. Silica-coated gold nanorods were purified and then characterized by TEM imaging and UV–vis absorbance spectroscopy. The average silica shell thickness for each of the five aspect ratios and five silica shell thickness are listed in Table S3. UV–vis absorbance spectra of silica-coated gold nanorods in ethanol (EtOH) (not shown) do not exhibit nanorod aggregation.

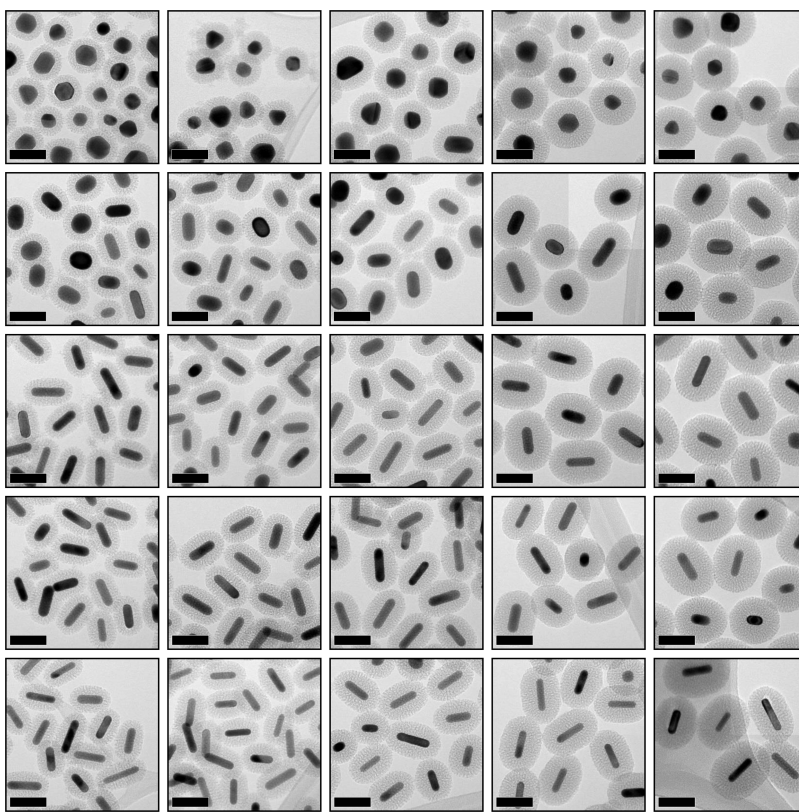


**Figure 3.** TEM images of azide-functionalized silica-coated gold nanorods with increasing silica shell thickness left to right (11, 14, 17, 22, and 26 nm) and with increasing aspect ratio top to bottom (AR 1.1, 2.0, 2.7, 3.7, and 4.4). Scale bars = 50 nm.

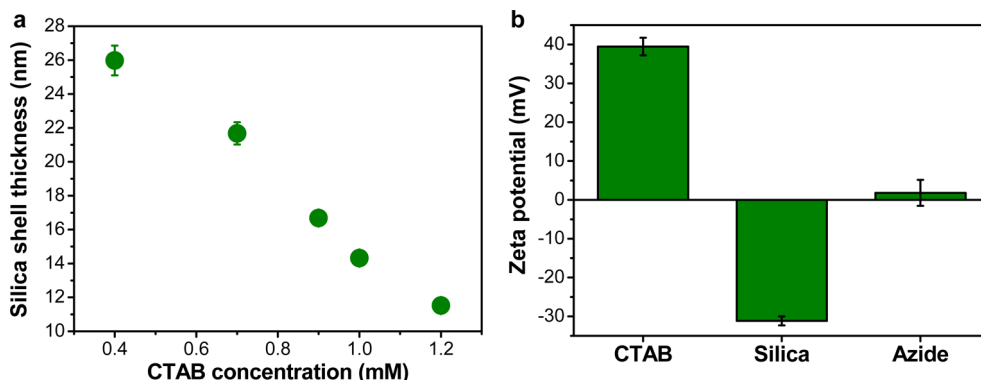


**Figure 4.** (a) CTAB concentration versus average silica shell thickness for the five shell thicknesses used. (b)  $\zeta$ -Potentials of AR 2.7 gold nanorods coated in CTAB, a 22 nm thick silica shell and functionalized with the azide.

Only small shifts in plasmon maxima, less than 10 nm between different shell thicknesses, are observed (Table S4).

Silica-coated gold nanorods were then functionalized with an organic azide, which could participate in the cycloaddition reaction to bind IRDye 800CW DBCO to the surface.<sup>39</sup> The azide, 3-azidopropyltrimethoxysilane, was prepared from 3-chloropropyltrimethoxysilane via a modification of the published Finkelstein reaction (Figure S1).<sup>40</sup> Heating 3-chloropropyltrimethoxysilane and sodium azide in *N,N*-dimethylformamide (DMF) yielded the azide product in greater than 90% yield, as assessed by gas chromatography/mass spectrometry (not shown). The reaction mixture was then extracted

into hexanes, which yielded a solution of pure azide in DMF and was stable at room temperature. Azide functionalization was carried out by simply adding the azide, in DMF, to a solution of the silica-coated gold nanorods in EtOH. Complete silane condensation on the silica surface was further driven by heating the solutions. After functionalization, the gold nanorod solutions were purified by centrifugation multiple times to ensure complete removal of excess azide and were then dispersed in MeOH in preparation for IRDye conjugation.

Azide-functionalized gold nanorods were characterized by UV-vis absorbance,  $\zeta$ -potential measurements,

and Fourier transform infrared spectroscopy (FTIR). UV-vis absorbance spectra of azide-functionalized, silica-coated gold nanorods in MeOH (not shown) show no nanorod aggregation. However, due to heating, multiple centrifugation steps, and dispersion in various solvents, the average nanorod plasmon maxima shifts to 535, 650, 720, 776, and 823 nm for AR 1.1, AR 2.0, AR 2.7, AR 3.4, and AR 4.4, respectively. Only small shifts in absorbance maxima, less than 18 nm between different shell thicknesses, are observed (Table S5).  $\zeta$ -Potential measurements confirm functionalization of the gold nanorods (Figure 4b). CTAB gold nanorods are positively charged, and after silica coating and purification, the surface charge is negative. Upon azide functionalization, the surface charge of the nanorods approaches zero due to the presence of the neutral azide. Further confirmation of azide functionalization is demonstrated by FTIR. These nanorods were purified by dialysis and extra centrifugation steps to ensure that all free azide was removed before FTIR analysis. An azide stretch is visible at  $2100\text{ cm}^{-1}$  in a spectrum of azide-functionalized nanorods, further confirming azide functionalization (Figure S2).

IRDye was attached to azide-functionalized, silica-coated gold nanorods *via* a copper-free click reaction. The concentration of an IRDye stock solution was determined by absorbance at 779 nm ( $\epsilon = 300\,000\text{ M}^{-1}\text{cm}^{-1}$  in MeOH).<sup>28</sup> Then, IRDye was added to azide-functionalized silica-coated gold nanorods in MeOH. A click reaction can occur in 45 min, but the IRDye/nanorod solutions were mixed overnight to ensure maximum IRDye attachment.<sup>39</sup> The solutions were centrifuged, the supernatant was removed, and the pellets containing IRDye-loaded nanorods were suspended in MeOH. The supernatants were centrifuged a second time to completely remove any residual nanorods. Fluorescence emission peak area of each supernatant was measured, and dye loading was calculated from a calibration curve of IRDye peak area *versus* concentration. We assume dye molecules bound = original – free. Originally, 200 dye molecules were added per particle, and dye loading was  $\sim 80\%$  with 160 IRDye molecules/nanorod. This allows for an average dye–dye distance of 9 nm or greater on the nanoparticle surface, reducing potential dye–dye interactions during fluorescence studies.

**Plasmon-Enhanced Fluorescence.** The complex physics of a quantum emitter coupled to a metal nanoparticle has been explored in the literature.<sup>41–45</sup> Unfortunately, these treatments do not completely address the situation here. Molecular fluorescence is well understood and simply described by eq 1, where quantum yield or quantum efficiency ( $Q$ ) is the ratio of the radiative decay rate ( $k_{\text{rad}}$ ) to the total of all contributions to excited-state decay, both radiative and nonradiative ( $k_{\text{nr}}$ ).

$$Q = \frac{k_{\text{rad}}}{k_{\text{rad}} + k_{\text{nr}}} = k_{\text{rad}} \cdot \tau \quad (1)$$

Alternatively,  $Q$  can be calculated from knowledge of the  $k_{\text{rad}}$  and fluorescence lifetime ( $\tau$ ). The fluorescence lifetime (eq 2) is the average time a fluorophore spends in the excited state before it relaxes to the ground state and is the inverse of the sum of the decay rates of all the relaxation pathways ( $k$ ).<sup>46</sup>

$$\tau = \frac{1}{k_{\text{rad}} + k_{\text{nr}}} = \frac{1}{k} \quad (2)$$

For a free fluorophore in solution, nonradiative decay is caused by processes such as internal conversion, intersystem crossing, or collisional quenching.<sup>46</sup> However, when a fluorophore is attached to the surface of a nanorod, the relaxation dynamics will become quite complex. Both radiative and nonradiative decay can be changed when there is coupling near a plasmonic surface. The presence of the metal particle provides a continuum of states to which the molecule can couple. The potential decay pathways become more numerous, complicating the emission dynamics which define the new fluorescence lifetime ( $\tau_0$ ) and new total decay rate ( $k_0$ ) shown in eq 3. We can incorporate changes in free dye  $k_{\text{rad}}$  and  $k_{\text{nr}}$  by adding the new terms  $K_{\text{rad}}$  and  $K_{\text{nr}}$ , where the former refers to plasmon-induced radiative rate enhancement and the latter the nonradiative dye–rod interactions driven by energy dissipation to the nanorod continuum states. Finally, there can potentially be associated dye–surface interactions ( $k_s$ ) or dye–dye fluorescence coupling ( $k_{\text{dd}}$ ) on the nanoparticle surface that may also modify fluorophore dynamics.

$$\tau_0 = \frac{1}{k_{\text{rad}} + k_{\text{nr}} + K_{\text{rad}} + K_{\text{nr}} + k_s + k_{\text{dd}}} = \frac{1}{k_0} \quad (3)$$

Depending on the nanoparticle–fluorophore system used, these processes may result in a change in the fluorescence lifetime.<sup>21</sup> All these interactions must be taken into account before making conclusions about changes in fluorescence intensity. By combining steady-state intensity measurement data with lifetime measurement data, it is possible to obtain a comprehensive picture of observed changes in fluorescence relative to free dye.

If we consider the basic physics involved, we can bound our observational expectations. The general approximate expression for the one-photon absorption cross section,  $\sigma^{(1)}(\omega)$ , for a dipolar quasi-two-level fluorophore excited at frequency ( $\omega$ ) is shown in eq 4, where  $\mu$  is the transition dipole of the emitter,  $\rho(\omega)$  is the molecular density of states (effectively the absorption spectral shape), and  $n$  and  $c$  are the index of refraction and speed of light, respectively.

$$\sigma_{\text{IRDye}}^{(1)}(\omega) = \frac{4\pi^2\omega}{nc} |\mu_{\text{IRDye}}|^2 \rho(\omega_{\text{IRDye}}) \quad (4)$$

The full transition rate  $R$  is defined by eq 5, where  $I_{\text{exc}}$  is the excitation field intensity:

$$R_{\text{IRDye}} = \sigma_{\text{IRDye}}^{(1)}(\omega) I_{\text{exc}} \quad (5)$$

Our question here is simply, is one or both of these molecular quantities in eq 5 modified by dye–nanorod coupling?<sup>47,48</sup> The plasmon-induced E-field enhancement makes  $I_{\text{exc}}$  much larger, which of course would drive a larger excited-state population of the dye *via R*. If that was the dominant effect, the plasmon-induced/enhanced population of the excited state would result in detection of enhanced fluorescence emission, but there need be no change of the observed dye kinetics (the radiative rate would not be modified). On the other hand, if the cross-section,  $\sigma^{(1)}$ , is affected, the actual radiative rate will be changed with that change manifest in the observed decay dynamics of the emitter.

A formalism describing the field interactions involved has been developed in the literature.<sup>49–52</sup> It has been shown that the decay rate,  $K_{\text{rad}}$ , of a dipolar emitter near a plasmonic structure can be written as eq 6, where  $k_{\text{rad}}$  is the radiative rate of the free dye. The second term on the right contains the imaginary part of dipolar coupling scaled by the amplitude of  $\mu$  and the field free space wavevector  $\vec{k}$ .<sup>49</sup>

$$\frac{K_{\text{rad}}}{k_{\text{rad}}} \approx 1 + \frac{3}{2} \text{Im} \frac{\vec{\mu} \cdot \vec{E}(\vec{r}, \omega_0)}{|\mu|^2 \vec{k}^3} \quad (6)$$

The complete analytical solution to this problem requires full multipole expansion of the electric field,  $\vec{E}(\vec{r}, \omega_0)$  and is very complex, but the result gives rise to the two key dynamic observables of the system: the well-known Förster transfer process for the plasmon-induced nonradiative contribution and a complex radiative contribution driven by the “Drude metal” polar nature of the plasmon resonance. In general, the nonradiative rate modification results from energy dissipation of the emitter to the nanorod *via* dipole–dipole coupling. The radiative contribution is driven by the polarizability of the total system, dye coupled to rod, and its impact on the transition dipole. While the components of radiative enhancement are hard to discern independently, we will show that its signature is observed in our lifetime data.

**Fluorescence Studies.** Fluorescence intensity analysis of IRDye-loaded, silica-coated, gold nanorods was first carried out by steady-state measurements. The solutions were excited at the dye absorbance maximum (779 nm), and fluorescence emission was measured from 785 to 875 nm. Comparison of the fluorescence emission curves to curves of free IRDye shows no change in shape or emission maxima (fluorescence spectra are not shown). No emission was detected from silica-coated gold nanorods alone, without dye, suggesting that scattering from the nanorods alone is minimal. Since each of the samples demonstrated variation in dye loading, it was necessary to calculate separate expected emission. A calibration curve of fluorescence peak area versus IRDye concentration

was constructed. The relative fluorescence intensity of IRDye-loaded nanorods was calculated by dividing the measured peak area by the expected peak area. Since gold nanorods strongly absorb in regions of IRDye absorption/emission and their extinction can be orders of magnitude stronger than IRDye, measured fluorescence emission can be reduced. This is called the inner-filter effect, and it is necessary to correct for this effect in solution-based measurements. The corrected emission intensity was calculated from eq 7, where  $I_{\text{corr}}$  is the corrected emission intensity,  $I_0$  is the relative fluorescence intensity calculated from steady-state measurements, and  $\text{OD}_{\text{ex}}$  and  $\text{OD}_{\text{em}}$  are the optical density values for each dye/nanoparticle solution at 779 and 794 nm, respectively.<sup>46</sup>

$$I_{\text{corr}} = I_0 \times 10^{(\text{OD}_{\text{ex}} + \text{OD}_{\text{em}})/2} \quad (7)$$

Equation 7 does not account for light scattering, which also occurs when the surface plasmon resonance is excited. The scattering contribution from gold nanorods in this size range has been measured for 800 nm incident light, and the maximum contribution of scattering to the total extinction as a function of aspect ratio was 9, 15, 10, 6, and 5% for aspect ratios of 2.5, 3.0, 4.0, 4.5, and 5.1, respectively.<sup>53</sup> Therefore, 85–95% of the light is absorbed by the nanorods rather than scattered. Consequently, the likelihood of scattered light being reabsorbed by nearby dye molecules is quite low and should not be a significant contribution to detected fluorescence emission.

The results of the steady-state fluorescence measurements are shown in Figure 5. The line cuts show intensity plotted relative to free IRDye as a function of silica shell thickness and plasmon band maximum (Figure 5a–e). Both distance and plasmon wavelength dependent changes in fluorescence are observed. At the plasmon maximum furthest away from the emission wavelength (535 nm), where there is minimal spectral overlap with the emission of IRDye, there is only slight intensity enhancement observed. A decrease in fluorescence is observed with decreasing silica shell thickness (Figure 5a). This is consistent with increasing nonradiative relaxation ( $K_{\text{nr}}$ ) as the fluorophore gets closer to the continuum states of the nanorod. When there is stronger overlap between the plasmon band and IRDye absorbance/emission, fluorescence intensity enhancement becomes more apparent (Figure 5b–e). Interestingly, at these plasmon maxima, the maximum fluorescence intensity is observed at approximately 17 nm. The strongest enhancement is observed when the plasmon maximum of the nanorods is 776 nm, near resonant with IRDye absorption, resulting in an approximately 10-fold increase in fluorescence intensity. The trends and scale of the fluorescence intensity are more clearly observed in Figure 5f, which is a three-dimensional, two-tier contour plot of emission intensity as a function of silica

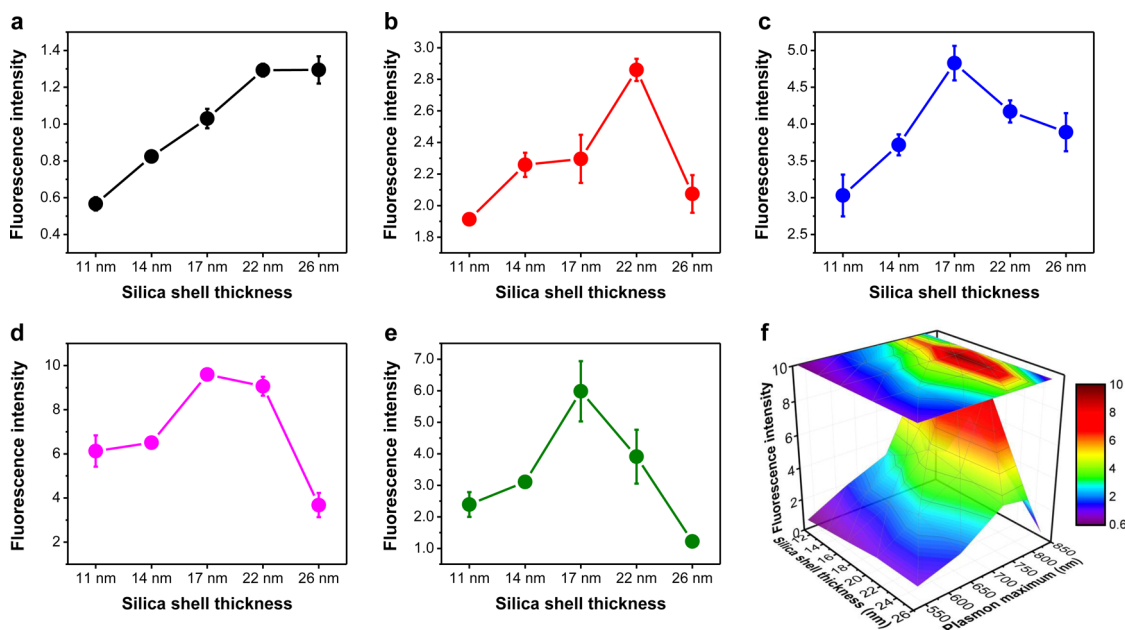


**Figure 5.** Steady-state fluorescence intensity of IRDye bound to gold nanorods relative to free IRDye corrected for the inner-filter effect. Intensity as a function of silica shell thickness with plasmon band maxima located at (a) 535 nm, (b) 650 nm, (c) 720 nm, (d) 776 nm, and (e) 823 nm. (f) Two-tier contour plot of fluorescence intensity as a function of silica shell thickness and plasmon maximum.

shell thickness and plasmon maximum. The “hotspot” of fluorescence intensity (the dark red area) occurs in the region from 14 to 22 nm silica shell thickness between plasmon maxima at 750 and 800 nm.

A possible concern is the contribution of scattering by the nanorods to an “apparent” fluorescence enhancement, either directly or by reabsorption of scattered photons by dyes in the sample. At aspect ratio 3.0, where there would be ~15% scattering<sup>53</sup> (Figure 5c), we observe decreased fluorescence intensity compared to aspect ratio 4.5, where there would be ~6% scattering (Figure 5e).<sup>53</sup> This supports the notion that increased dye excitation due to light scattering from the nanorods is not the major contributor to dye emission.

The observed increases in fluorescence intensity can be attributed to strong coupling between the fluorophores and the plasmonic structure, but how the changes are manifest are not obvious. As noted, there can be several possible reasons for an increased detection of emission. There can be a change of the emission cross section (radiative decay rate) relative to the nonradiative decay, or there simply could be an effective increase in excited-state population which result in no change in radiative emission dynamics. We can explore these questions more effectively by examining the system’s time-resolved fluorescence characteristics. Time-resolved photoluminescence (TRPL) measurements were carried out to determine fluorescence lifetime as a function of silica shell thickness and plasmon maximum. In the TRPL measurements, the dye/nanorod solutions were excited

with a 740 nm pulsed laser and emitted photons were collected in the region from 795 to 805 nm. An emission filter was used to limit the detected emission bandwidth to 10 nm; we note that only emission from IRDye is observed.

The data from TRPL measurements, that is, decay curves of time versus emission, are shown in Figure 6. The decay of free IRDye (Figure 6a) exhibits a single exponential decay while nearly all curves of IRDye bound to silica-coated gold nanorods, especially in the strongly coupled regions, exhibit multiexponential decays (Figure 6b–f). This indicates, of course, that there are new and possibly multiple pathways of decay present in the dye–nanorod system that are not present when IRDye is free in solution as implied by eq 3. In all cases, decay appears faster as silica shell thickness decreases. This is consistent with increased  $K_{nr}$ . As stated, an increase in the decay rate is expected due to the higher electromagnetic field strength induced at the nanorod surface, resulting in potentially a larger *emission cross section*, but there will also be more efficient nonradiative Förster coupling (which would also lead to much faster decay) when there is stronger spectral overlap between the plasmon band of the nanorods and IRDye absorbance/emission. Comparison of the fluorescence intensity results with the decay dynamics suggests that, when the plasmon is far off the emission resonance (Figure 6b), the increase in “nonradiative” rate,  $K_{nr}$ , drives evolution of the decay dynamics. As we space the fluorophore farther away from the rod core ( $\geq 22$  nm), we see dynamics consistent with the free dye. It is interesting to note that the

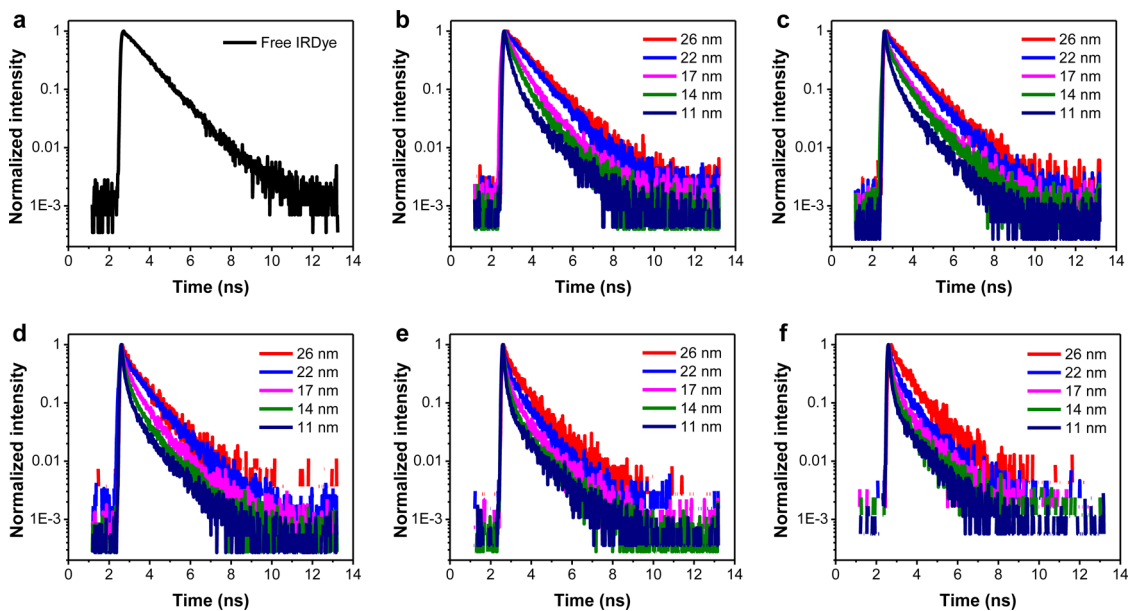


**Figure 6.** Fluorescence decay curves of (a) free IRDye and IRDye bound to gold nanorods as a function of silica shell thickness with plasmon band maxima located at (b) 535 nm, (c) 650 nm, (d) 720 nm, (e) 776 nm, and (f) 823 nm.

detected intensity at the largest distance is still larger than the free dye. This could signify a pure  $R_{\text{IRDye}}$  contribution at long distance (*i.e.*, a pure population enhancement). Near resonance (Figure 6e), the plasmon–fluorophore interaction comes strongly into play. Interestingly, if one focuses on the 22–26 nm spacing, the lack of large change in decay rates between (e) and (f) suggests that our enhancement is primarily radiative. Here, there is a large difference in absorptive behavior (Figure 2b) but no substantial change in kinetics.

The decay of the excited state of an isolated molecule to the ground state can be generally described by a single exponential, eq 8, where intensity ( $I$ ) is plotted as a function of the initial intensity ( $A$ ), time ( $t$ ), and the fluorescence lifetime.

$$I(t) = Ae^{-t/\tau} \quad (8)$$

The free dye exhibits this behavior, and using this equation, the lifetime of free IRDye was calculated to be 1.12 ns (this is close to the value of our maximum lifetimes at 26 nm shell thickness and far off resonance). However, a single exponential did not fit the majority of the decay curves. For simplicity, we fit the data to a biexponential decay (eq 9), where  $A_1$  and  $A_2$  are the initial intensities from the “fast” and “slow” components of fluorescence decay, respectively, and  $\tau_1$  and  $\tau_2$  are their respective fluorescence lifetimes. We note that this functional form generated the best fits in nearly every case.

$$I(t) = A_1 e^{-t/\tau_1} + A_2 e^{-t/\tau_2} \quad (9)$$

The fast and slow fluorescence lifetimes as a function of silica shell thickness and plasmon maximum are shown as contour plots in Figure 7. In the fast

component, both decreasing silica shell thickness and increasing plasmon/IRDye spectral overlap result in a very strong and abrupt reduction in the fluorescence lifetime (Figure 7a). As discussed above, the degree of spectral overlap can impact both radiative and nonradiative processes. The rather weak spectral resonance dependence suggests that the driver is primarily radiative. As mentioned above, there are rather large changes in fluorescence enhancement from 720 to 823 nm, but the kinetics changes are modest. The only region where we see the calculated lifetime is the same as free IRDye with nanorods absorbing at 535 nm and when silica shell thickness is greater than 20 nm. If we directly compare the fast and slow regimes, the trend of shell thickness and spectral overlap is similar, but the changes in lifetime are much more gradual in the slow component. Interestingly, the region of strongest reduction in fluorescence lifetime is not where maximum fluorescence intensity is observed. This indicates that the observed intensity enhancements cannot be completely attributed to an increase in the radiative decay rate  $K_{\text{rad}}$  (eq 3) but is a complex interplay of all the processes involved. Such lifetime changes are inconsistent with scattering as the main mechanism for increased light emission. We would expect that, at distances less than 20 nm, there is a simultaneous increase in the nonradiative decay rate that leads to the smaller increase in fluorescence intensity at these distances. This demonstrates the complexity of plasmon-enhanced fluorescence—it cannot simply be described as increased radiative decay rates near a plasmonic structure. Both distance and plasmon maximum are important factors in the changing decay rates and measured fluorescence lifetimes.

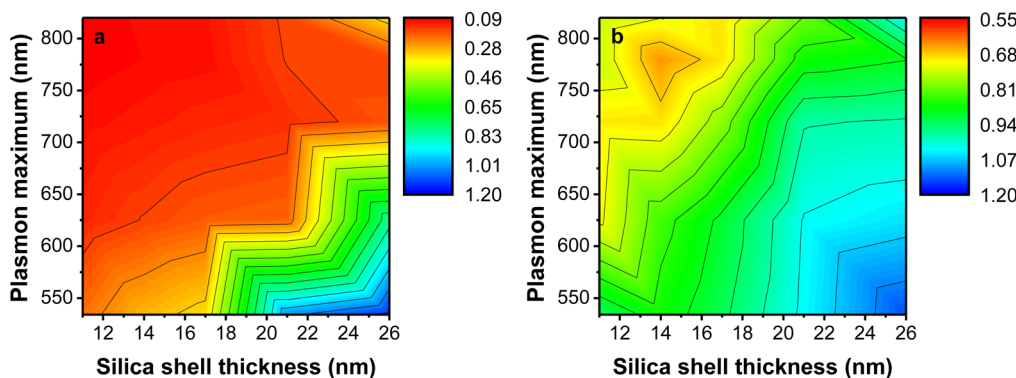


**Figure 7.** Contour maps showing fluorescence lifetimes (ns) of IRDye bound to silica-coated gold nanorods. Lifetimes were calculated from eq 5 giving two lifetime values, one “fast” and one “slow”. The (a) faster and the (b) slower lifetime components are plotted as a function of silica shell thickness and plasmon band maximum. The lifetime of free IRDye is 1.12 ns.

The percent of the slow component of the fluorescence lifetime decay is shown in Figure 8. The data show some interesting trends. For example, at the thick shell limit (26 nm), we see what is likely the pure plasmonic contribution mediated by its dependence on the orientation of each dye’s molecular transition dipole relative to the longitudinal plasmonic axis. At the other limit ( $\leq 14$  nm), nonradiative contributions become more important, but they clearly compete with the other plasmon-enhanced processes (*vide supra*). We note that the slow component is generally a significant fraction of the total emission dynamics and has both plasmonic and shell thickness dependence to its dynamics, so it cannot simply be attributed to unbound IRDye in solution.

These results suggest that there are possibly two distinct environments that the fluorophores experience on the nanoparticle surface. One possibility is the faster lifetime results from more strongly coupled species, whereas the slower lifetimes come from more weakly coupled dye molecules. Another reason for multiple apparent environments is nonrandom dye orientation and positions. We assume that orientation of IRDye molecules on the surface is random, but this may not be the case. It is possible that we are observing the effect of IRDye location (*i.e.*, fluorophores attached at the nanorod ends *versus* the rod sides). Dyes tethered near the ends of the rods would experience very different field strengths and could behave differently compared to dyes attached near the rod shaft center.<sup>49,54</sup> However, definitive experiments on the effect of end *versus* side dye loading on fluorescence behavior is beyond the scope of this work. A potential complicating factor is the possibility that IRDye could be loaded in the shell pores and therefore not at unique distance away from the metal. However, the pore size with this coating method is 2–2.5 nm,<sup>55,56</sup> and the IRDye diameter is approximately 2 nm.<sup>11</sup> With the additional reduction in pore size due to azide functionalization expected, it is unlikely that a significant fraction of IRDye would diffuse deep into the pores.

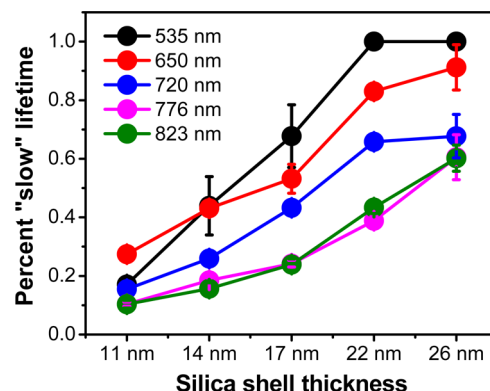


**Figure 8.** Percent of the slow component of the fluorescence lifetime as a function of silica shell thickness and plasmon band maximum.

**Dye—Nanoparticle Interactions.** Molecular fluorescence can be altered by simply changing the local environment surrounding a fluorophore.<sup>11,21</sup> It was therefore necessary to account for any possible dye—nanoparticle interactions such as dye—surface or dye—dye interactions that may have occurred, apart from an “antenna-like” or other plasmonic coupling. IRDye was attached to mesoporous silica nanoparticles (MSNs) that did not contain any gold cores to determine whether IRDye attachment to a silica surface resulted in any change in fluorescence. Azide-functionalized MSNs were prepared following the same Stöber synthesis and azide functionalization methods used for silica coating and functionalization of gold nanorods (Figure 9a). The as-synthesized MSNs are about 36 nm in diameter and show mesoporosity similar to the silica-coated gold nanorods.

Fluorescence of IRDye bound to MSNs was monitored via TRPL and steady-state measurements. TRPL measurements of IRDye-loaded MSNs and IRDye with the azide demonstrate single exponential decay behavior similar to free IRDye (Figure 9b). Calculated fluorescence lifetimes are shown in Table 1. The fluorescence lifetime of IRDye bound to the azide and the silica surface show only slight increases compared to

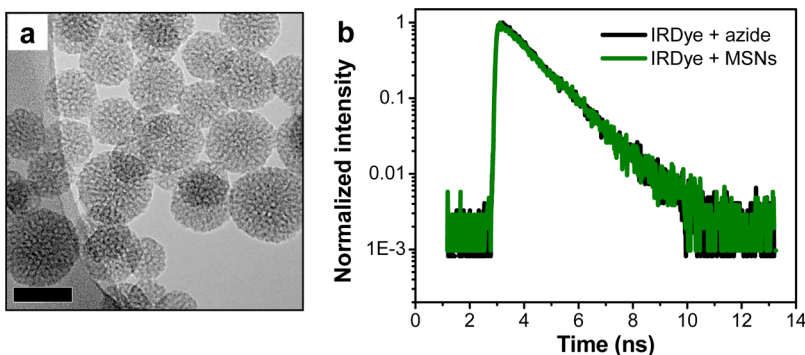


Figure 9. (a) TEM image of MSNs  $36 \pm 9$  nm. Scale bar = 50 nm. (b) Fluorescence decay curves of IRDye bound to the azide and MSNs.

**TABLE 1. Fluorescence Lifetime and Steady-State Intensity of IRDye Bound to Azide and MSNs**

sample	lifetime (ns)	steady-state intensity
IRDye	$1.12 \pm 0.02$	
IRDye + azide	$1.19 \pm 0.03$	
IRDye + MSNs	$1.24 \pm 0.04$	$1.04 \pm 0.02$

free IRDye. This small increase may be attributed to solvent properties or the change in refractive index near a silica surface. In addition, there is no change in steady-state fluorescence intensity compared to free IRDye (Table 1), which confirms that the slight increase in lifetime with the MSNs is not significant. These results demonstrate that simply binding IRDye to the silica surface does not significantly change fluorescence behavior.

Interactions between dye molecules on a surface can also modify fluorescence behavior, resulting in fluorescence quenching. At short dye separations, Förster resonance energy transfer can occur between neighboring fluorophores where a donor fluorophore transfers energy to an acceptor *via* nonradiative coupling, resulting in fluorescence quenching. This effect is dependent on the separation and degree of spectral overlap between neighboring fluorophores, and it is generally more pronounced when there is strong local dye concentration (*i.e.*, on a nanoparticle surface).<sup>57</sup> It is therefore necessary to limit dye loading on a nanoparticle to avoid issues of quenching which can result in decreased fluorescence lifetimes and steady-state intensity relative to free dye.

The effect of dye–dye separation on fluorescence behavior was investigated by changing the number of IRDye molecules loaded on the surface of silica-coated gold nanorods. AR 1.1 gold nanorods with a plasmon maximum at 535 nm were synthesized and coated with 33 nm thick silica (Figure 10 inset). The nanoparticles were loaded with varying amounts of IRDye to give estimated dye–dye separations ranging from 6 to 22 nm. Steady-state fluorescence analysis of these samples reveals that below 9 nm dye–dye separation

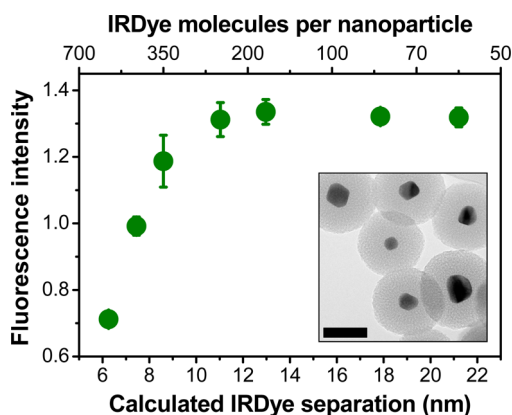


Figure 10. Steady-state fluorescence intensity relative to free IRDye as a function of dyes per nanoparticle or calculated separation between IRDye molecules. Inset is an image of AR 1.1 nanorods with 33 nm silica shells. Scale bar = 50 nm.

( $\sim 275$  dyes/nanoparticle), a significant decrease in fluorescence intensity occurs (Figure 10). However, at separations at or above 9 nm, the fluorescence intensity levels off due to the reduced interactions between neighboring fluorophores. Based on this result, IRDye loading was limited in all experiments to give separations at 9 nm or greater. This prevented any dye–dye interactions. Therefore, the observed changes in fluorescence of IRDye bound to silica-coated gold nanorods can only be due to plasmonic interactions not dye–dye or dye–surface interactions. We note that Wang *et al.* has modeled donor–acceptor energy transfer mediated by plasmonic coupling. Their work suggests that the plasmonic interaction is competitive with conventional Förster processes.<sup>58</sup>

**Comparison to Relevant Work.** Halas *et al.* have published several key papers on the photophysical properties of near-infrared-absorbing dyes in the presence of plasmonic nanoparticles.<sup>11,24,59</sup> In ref 24, her group demonstrated that near-infrared absorbing dyes near a plasmonic nanoparticle exhibited increased fluorescence quantum yield (up to 50-fold) for the case of a nanoparticle with a large scattering cross section and a plasmon maximum near the emission energy of the

dye.<sup>24</sup> In ref 11, Halas *et al.* found that the steady-state fluorescence emission of IRDye (called IR800) was enhanced by 9-fold on gold nanorods bearing an 8 nm protein layer, and that the fluorescence decay of the dye on the nanoparticle exhibited shorter lifetimes compared to free dye.<sup>11</sup> In ref 59, Halas *et al.* placed IRDye (called IR800 again) in a thin silica layer between a gold core and a gold shell, with the dye emission maximum resonant with a plasmon band maximum. The Halas group found a steady-state fluorescence enhancement by 16-fold for IRDye, comparing the gold–silica precursor seed to the final gold–silica–gold nanostructure, with the dyes approximately 4–10 nm away from the inner gold core.<sup>59</sup>

As Wang has pointed out,<sup>54</sup> the plasmonic field can alter both radiative and nonradiative decay rates in nearby molecules, even though it is frequently assumed that the nonradiative rate is not changing upon molecular adsorption onto a spacer layer on top of a plasmonic nanoparticle. In general, distances  $\sim$ 10 nm from the metal surface and plasmon peak positions between the absorption and emission maximum of the dye are considered optimal to observe plasmon-enhanced fluorescence.<sup>54</sup> Halas *et al.* have also suggested that, when the plasmon band is between absorbance and emission, enhancement is maximized.<sup>59</sup> In our case, IRDye's absorption and emission maxima are so close together that no plasmon band is “between” them; nonetheless, the nanorods that give the largest fluorescence enhancement are indeed the ones with a plasmon maximum that overlaps the molecular bands.

In addition, our fine gradation of silica shell thicknesses allows us to pinpoint the “best” spacer thickness at 17 nm. We find multiexponential fluorescence decays that show fast components for dyes on plasmonic nanoparticles, but these components vary as a function of silica shell thickness and plasmon band maximum in a complex manner. Quantum mechanical calculations of relative radiative and nonradiative decays for a dye molecule near a gold “nanorod” (which is taken as two spheres next to each other) show that, for a constant size of nanorod, moving the dye from

5 to 20 nm away increases both radiative and nonradiative rates from 5–15 nm, but at  $\sim$ 15 nm away, the nonradiative decay rate change turns off, and the radiative rate continues to increase, giving a higher relative brightness of emitted light from the dye.<sup>60</sup> The distance at which the behavior changes, 15 nm, is identical to what we find in our data (*vide supra*). A very recent report finds 1000-fold fluorescence enhancement of dyes near single gold nanorods in single-molecule experiments, especially when the plasmon is resonant with the laser and dye emission maximum, as observed here; the larger enhancements could be due to individual dye binding events near the ends of gold nanorods, a process that is not directly resolved in our data.<sup>61</sup>

## CONCLUSIONS

We have observed distance and plasmon wavelength dependent fluorescence of IRDye 800CW DBCO bound to silica-coated gold nanorods. Steady-state measurements demonstrate wavelength and distance dependent fluorescence emission with approximately 10-fold maximum fluorescence intensity enhancement observed in the fluorescence hotspot. The presence of multiexponential decay in the time-resolved measurements indicates that there were multiple decay pathways present in our system which are consistent with enhanced radiative and nonradiative contributions. A strong reduction in fluorescence lifetime is observed with decreasing silica shell thickness and when there is strong spectral overlap between nanorod plasmon band and IRDye absorption/emission. Control experiments confirm that the observed changes in fluorescence are due to plasmonic interactions, not simply attachment to surface. In addition, limiting IRDye loading assures minimal dye–dye interactions on the nanorod surfaces. Together, these results reveal that plasmon–fluorophore coupling, resulting in fluorescence intensity enhancement, is a complex process. Nevertheless, enhancement of low quantum yield fluorophores *via* coupling to plasmonic nanoparticles remains a viable option to increase their potential for biological applications.

## METHODS

**Materials.** Cetyltrimethylammonium bromide, gold tetrachloroaurate ( $\text{HAuCl}_4 \cdot 3\text{H}_2\text{O}$ ), sodium borohydride ( $\text{NaBH}_4$ ), silver nitrate ( $\text{AgNO}_3$ ), ascorbic acid, sodium hydroxide ( $\text{NaOH}$ ), tetraethylorthosilicate, ethanol ( $\text{EtOH}$ ), indocyanine green dye, 3-chloropropyltrimethoxysilane, sodium azide, sodium iodide, *N,N*-dimethylformamide (DMF), and methanol ( $\text{MeOH}$ ) were purchased from Sigma-Aldrich (USA). IRDye 800CW DBCO was purchased from LI-COR Biosciences. All chemicals were used as received without further purification.

**Synthesis of Gold Nanorods.** Gold nanorods were prepared using our seed-mediated growth procedure.<sup>33</sup> First, 9.75 mL of 0.1 M CTAB was added to 0.25 mL of 0.01 M  $\text{HAuCl}_4 \cdot 3\text{H}_2\text{O}$ ,

and the solution was kept stirring for 10 min. Next, 0.043 g of  $\text{NaBH}_4$  was added to 10 mL of ice cold deionized water. Immediately, the 0.1 M  $\text{NaBH}_4$  solution was mixed and 1 mL of it was transferred into a second tube containing 9 mL of ice cold deionized water. Then, 0.60 mL of the 0.01 M  $\text{NaBH}_4$  was quickly added to the solution of CTAB and  $\text{HAuCl}_4$  forming gold seeds. The gold seed solution was stirred for 10 min and then aged for 1 h before use.

Five, 500 mL batches of CTAB-coated gold nanorods were prepared. A growth solution containing 475 mL of 0.1 M CTAB, 25 mL of 0.01 M  $\text{HAuCl}_4 \cdot 3\text{H}_2\text{O}$ , and varied amounts of 0.01 M  $\text{AgNO}_3$  (0.10, 1.25, 2.50, 3.75, or 5.50 mL) was prepared. Increasing amounts of  $\text{AgNO}_3$  resulted in higher aspect ratio nanorods formed. Next, 2.75 mL of 0.1 M ascorbic acid was added to the

growth solutions, which turned colorless upon addition of ascorbic acid. Then, 0.6 mL of gold seed solution was added under vigorous stirring. The solutions began changing color after 15 min, then stirring was slowed, and the solution was allowed to age overnight (16 h at 27 °C). The next day the gold nanorod solutions were purified *via* centrifugation at 13 500 rcf for 20 min, and the pellets were suspended in deionized water for further use.

Absorbance spectra were taken using a Cary 500 UV–vis spectrometer (Agilent, USA) to determine plasmon band maxima and nanorod concentration. Concentration of gold nanorod solutions was determined from calculated extinction coefficients at each plasmon maximum, which in turn had been calibrated using inductively coupled plasma atomic emission spectroscopy.<sup>62</sup> Transmission electron microscopy images were obtained on a JEOL 2100 cryo-TEM (JEOL, Japan). ImageJ analysis of TEM images (300 particles per sample) was carried out to determine average length, width, and aspect ratio.

**Silica-Coated Gold Nanorods.** Silica coating was carried out using a modified Stöber method.<sup>29</sup> CTAB concentration was tightly controlled during silica coating. After initial synthesis and purification, the gold nanorod solutions were centrifuged a second time at 11 200 rcf for 20 min. The supernatant was removed, and the pellets were separated to five tubes, each diluted to 10 mL for a final nanorod concentration of 1 nM. After two centrifugations, the concentration of CTAB was <0.01 mM. Then, 0.1 M CTAB was added to each of the five tubes to adjust the CTAB concentration to 0.4, 0.7, 0.9, 1.0, or 1.2 mM. The solutions were mixed overnight to allow the CTAB to equilibrate on the surface of the gold nanorods. Then, 40 μL of 0.1 M NaOH was added to adjust pH to 10.6, and the solutions were mixed for 30 min. Next, 90 μL of 20% TEOS in methanol was added, and the solutions were mixed for 20 h at room temperature. The nanorods were transferred to new centrifuge tubes and then purified *via* centrifugation at 8000 rcf for 20 min. The supernatant was removed, and the pellets were dispersed in 5 mL of EtOH.

**Synthesis of the Azide, 3-Azidopropyltrimethoxysilane.** Synthesis of the azide was carried out through modification of a previously published protocol.<sup>40</sup> Sodium azide (493 mg, 7.5 mmol) and sodium iodide (28 mg, 0.1875 mmol) were added to a 100 mL round-bottom flask followed by 20 mL of DMF. The suspension was stirred for 5–10 min, allowing the solids to dissolve. 3-Chloropropyltrimethoxysilane (1.25 g, 6.3 mmol) was added, and the reaction was capped and stirred for 12 h at 100 °C.

The compound was used as a solution in DMF isolated directly from the reaction mixture as follows. The crude mixture was filtered through Celite and the resulting solution layered with 80 mL hexanes. The biphasic mixture was stirred vigorously for 4 h, at which time the phases were separated and the hexanes fraction was concentrated to clear oil. The concentration of the azide was determined by <sup>1</sup>H NMR (400 MHz Varian Inova Ul400 spectrometer). The DMF layer was resubmitted to the above procedure until the hexanes layer no longer contained product. The resulting product was stable when diluted to 25% in DMF and was used without further purification.

**Warning:** While the alkyl azide did not exhibit shock or impact sensitivity, it should be noted that the reagent is unstable as a neat liquid, completely decomposing within 48 h at room temperature. While this has been a relatively safe reagent in our laboratory, this should not excuse anyone from exercising proper caution in its use.

**Azide Functionalization of Silica-Coated Gold Nanorods.** One hundred microliters of the azide (25% in DMF) was added to the silica-coated gold nanorods in EtOH. The solutions were heated overnight (10 h at 80 °C) to ensure complete functionalization of the surface. Purification was carried out *via* centrifugation at 10 000 rcf for 20 min. The solutions were centrifuged, the supernatant was removed, and the pellet was redispersed three times in MeOH to remove all excess azide. The azide-functionalized, silica-coated gold nanorods were characterized by UV–vis absorbance spectroscopy to determine concentration and plasmon maxima. The samples were all diluted to 0.8 nM for further characterization and IRDye attachment.

TEM image analysis was carried out with ImageJ with 300 particles measured per sample to determine average silica shell

thickness. ζ-Potentials of CTAB, silica-coated, and azide-functionalized gold nanorods were measured using a ZetaPals zeta-potential analyzer (Brookhaven, USA). In addition, a few samples of azide-functionalized silica-coated gold nanorods were purified by dialysis and three additional centrifugation steps to ensure removal of all free azide. Fourier transform infrared spectroscopy of these highly purified solutions was carried out using a PerkinElmer Spectrum 100 (PerkinElmer, USA) to confirm the presence of the azide on the surface.

#### IRDye Attachment to Azide-Functionalized Silica-Coated Gold Nanorods.

The concentration of an IRDye stock solution in MeOH was determined by measuring absorbance of IRDye ( $\epsilon = 300\,000\text{ M}^{-1}\text{cm}^{-1}$  in MeOH).<sup>28</sup> Then, 50 μL of 10 μM IRDye was added to 3 mL of 0.8 nM azide-functionalized silica-coated gold nanorods in MeOH. The IRDye/nanorod solutions were mixed overnight (>12 h) at room temperature for IRDye coupling. The solutions were centrifuged at 15 000 rcf for 20 min, the supernatant was removed, and the pellets containing IRDye-loaded nanorods were suspended in 3 mL of MeOH. The supernatants were spun a second time at 15 000 rcf for 20 min to completely remove any residual nanorods. Fluorescence emission peak area of each supernatant was measured to determine IRDye loading (see procedure below). Loading was calculated assuming dye molecules bound = original – free. Typically, dye loading was ~80% with 160 IRDye molecules/nanorod. All fluorescence analysis was carried out in MeOH with three samples of IRDye-loaded gold nanorods prepared and analyzed for each of the five aspect ratios and five silica shell thicknesses used. In addition, all sample containers with IRDye were covered with aluminum foil to reduce photobleaching.

**Steady-State Fluorescence Measurements.** Steady-state fluorescence measurements were carried out on a Fluoromax-3 (Horiba Scientific, Japan) to determine fluorescence enhancement and quenching. Fluorescence emission spectra of IRDye and IRDye/nanorod solutions were collected with excitation set at 779 nm and emission measured in the region from 785 to 900 nm. By beginning emission collection at 785 nm, gold nanorod scattering was minimal and the only fluorescence emission observed was due to IRDye fluorescence. Since each sample had varied dye loading, it was necessary to calculate expected fluorescence emission for each sample. A calibration curve of fluorescence peak area versus free IRDye concentration was constructed. The fluorescence intensity of IRDye-loaded nanorods was calculated by dividing the measured peak area by the expected peak area calculated from the calibration curve.

An inner filter correction was applied to obtain an accurate value for fluorescence intensity since gold nanorods strongly absorb at wavelengths of IRDye absorption/emission. Absorbance of the solutions of IRDye-loaded nanorods was measured at the excitation and emission wavelengths. The corrected emission intensity was calculated from eq 7.<sup>46</sup>

**Time-Resolved Photoluminescence Measurements.** TRPL measurements were carried out using a home-built correlated single-photon counting system at the Materials Research Laboratory, University of Illinois. The system uses a Becker and Hickel SPC-150 photon counting board to process signals with a silicon avalanche photodiode. The excitation source is a NKT Photonics pulsed supercontinuum source. In the TRPL measurements, the dye/nanorod solutions were excited with a 740 nm (10 nm bandpass), 6 ps pulse. The system impulse response is ~50 ps. Fluorescence emission was collected in the region from 795 to 805 nm. Because the emission filter used limited the emission wavelengths to 10 nm, gold nanorod scattering was minimal and the only emission observed was due to IRDye fluorescence. The data from TRPL measurements were used to construct a curve of time versus emission which exhibited multiexponential decay. The fit was calculated using Origin, and eq 9 to calculate the lifetimes present.<sup>46</sup>

**IRDye Attachment to Mesoporous Silica Nanoparticles.** MSNs were prepared following similar procedures used for silica coating and azide functionalization of gold nanorods. First, 400 μL of 0.1 M CTAB was diluted to 50 mL to give a final CTAB concentration of 0.8 mM. Then, 200 μL of 0.1 M NaOH was added. The solution was mixed for 30 min, then 450 μL of 20% TEOS in MeOH was added. The solution was aged for 20 h and was

purified via centrifugation at 8000 rcf for 20 min. The MSNs were suspended in EtOH (4 mL), and then 500  $\mu$ L of the azide (25% in DMF) was added. The solution was heated overnight at 80 °C (>10 h) and purified via centrifugation. IRDye attachment, steady-state fluorescence, and TRPL measurements were carried out as previously described with three separate samples of MSNs.

**IRDye Fluorescence as a Function of Separation between Fluorophores.** Gold nanorods (AR 1.1) were synthesized and coated with silica as previously described. The CTAB concentration was 0.3 mM during silica coating, resulting in 33 nm thick silica shell. Three milliliters of 0.5 nM gold nanoparticles were incubated overnight (>12 h) with initial IRDye ranging in concentration from 50 to 2000 dyes/particle. Surface area was calculated assuming the dimensions can be approximated by a sphere. These concentrations gave dye–dye separations ranging from 6 to 22 nm. Quantification of IRDye attachment and steady-state fluorescence intensity was carried out as previously described with three samples analyzed for each dye–dye separation distance measured.

**Calculation of IRDye Quantum Yield in MeOH.** Quantum yield of IRDye 800CW DBCO in MeOH was determined using indocyanine green as a standard reference (absorbance/emission maxima at 785/806 nm). Three solutions each of IRDye and indocyanine green were prepared with identical dye concentrations (0.2  $\mu$ M). Fluorescence emission was measured as previously described. Quantum yield of IRDye was calculated from eq 10, where  $Q_R$  is the quantum yield of the reference standard in MeOH, OD and OD<sub>R</sub> are the absorbance, and  $I$  and  $I_R$  are fluorescence emission peak areas of IRDye and the reference standard, respectively.<sup>46</sup>

$$Q = Q_R \frac{I}{I_R} \frac{OD}{OD_R} \quad (10)$$

**Conflict of Interest:** The authors declare no competing financial interest.

**Acknowledgment.** This material is based upon work supported by the National Science Foundation Graduate Research Fellowship Program under Grant Number DGE-1144245. We also thank the Thomas B. Rauchfuss group for the use of their Fourier transform infrared spectrometer and the Kenneth S. Suslick group for the use of their fluorometer. Transmission electron microscopy and time-resolved fluorescence measurements were carried out in the Frederick Seitz Materials Research Laboratory Central Facilities, University of Illinois.

**Supporting Information Available:** A table of calculated quantum yields of the dyes used and tables of gold nanorod characterization including length, width, aspect ratio, plasmon maxima, and silica shell thickness are included. Also, NMR and FTIR spectra confirming azide synthesis and functionalization. This material is available free of charge via the Internet at <http://pubs.acs.org>.

## REFERENCES AND NOTES

1. Lohse, S. E.; Murphy, C. J. The Quest for Shape Control: A History of Gold Nanorod Synthesis. *Chem. Mater.* **2013**, *25*, 1250–1261.
2. Nikoobakhsh, B.; El-Sayed, M. A. Preparation and Growth Mechanism of Gold Nanorods (NRs) Using Seed-Mediated Growth Method. *Chem. Mater.* **2003**, *15*, 1957–1962.
3. Murphy, C. J.; Thompson, L. B.; Chernak, D. J.; Yang, J. A.; Sivapalan, S. T.; Boulos, S. P.; Huang, J.; Alkilany, A. M.; Sisco, P. N. Gold Nanorod Crystal Growth: From Seed-Mediated Synthesis to Nanoscale Sculpting. *Curr. Opin. Colloid Interface Sci.* **2011**, *16*, 128–134.
4. El-Sayed, M. A. Some Interesting Properties of Metals Confined in Time and Nanometer Space of Different Shapes. *Acc. Chem. Res.* **2001**, *34*, 257–264.
5. Eustis, S.; El-Sayed, M. A. Why Gold Nanoparticles Are More Precious than Pretty Gold: Noble Metal Surface Plasmon Resonance and Its Enhancement of the Radiative and Nonradiative Properties of Nanocrystals of Different Shapes. *Chem. Soc. Rev.* **2006**, *35*, 209–217.
6. Link, S.; Mohamed, M. B.; El-Sayed, M. A. Simulation of the Optical Absorption Spectra of Gold Nanorods as a Function of Their Aspect Ratio and the Effect of the Medium Dielectric Constant. *J. Phys. Chem. B* **1999**, *103*, 3073–3077.
7. N'Gom, M.; Li, S.; Schatz, G.; Erni, R.; Agarwal, A.; Kotov, N.; Norris, T. B. Electron-Beam Mapping of Plasmon Resonances in Electromagnetically Interacting Gold Nanorods. *Phys. Rev. B* **2008**, *80*, 113411.
8. Norman, R. S.; Stone, J. W.; Gole, A.; Murphy, C. J.; Sabo-Atwood, T. Targeted Photothermal Lysis of the Pathogenic Bacteria, *Pseudomonas aeruginosa*, by Gold Nanorods. *Nano Lett.* **2008**, *8*, 302–306.
9. Nikoobakhsh, B.; Wang, J.; El-Sayed, M. A. Surface-Enhanced Raman Scattering of Molecules Adsorbed on Gold Nanorods: Off-Surface Plasmon Resonance Condition. *Chem. Phys. Lett.* **2002**, *366*, 17–23.
10. Sivapalan, S. T.; Vella, J. H.; Yang, T. K.; Dalton, M. J.; Swiger, R. N.; Haley, J. E.; Cooper, T. M.; Urbas, A. M.; Tan, L.-S.; Murphy, C. J. Plasmonic Enhancement of the Two Photon Absorption Cross Section of an Organic Chromophore Using Polyelectrolyte-Coated Gold Nanorods. *Langmuir* **2012**, *28*, 9147–9154.
11. Bardhan, R.; Grady, N. K.; Cole, J. R.; Joshi, A.; Halas, N. J. Fluorescence Enhancement by Au Nanostructures: Nanoshells and Nanorods. *ACS Nano* **2009**, *3*, 744–752.
12. Fu, Y.; Zhang, J.; Lakowicz, J. R. Plasmon-Enhanced Fluorescence from Single Fluorophores End-Linked to Gold Nanorods. *J. Am. Chem. Soc.* **2010**, *132*, 5540–5541.
13. Nepal, D.; Drummy, L. F.; Biswas, S.; Park, K.; Vaia, R. A. Large Scale Solution Assembly of Quantum Dot–Gold Nanorod Architectures with Plasmon Enhanced Fluorescence. *ACS Nano* **2013**, *7*, 9064–9074.
14. Darvill, D.; Centeno, A.; Xie, F. Plasmonic Fluorescence Enhancement by Metal Nanostructures: Shaping the Future of Bionanotechnology. *Phys. Chem. Chem. Phys.* **2013**, *15*, 15709–15726.
15. Gandra, N.; Portz, C.; Tian, L.; Tang, R.; Xu, B.; Achilefu, S.; Singamaneni, S. Probing Distance-Dependent Plasmon-Enhanced Near-Infrared Fluorescence Using Polyelectrolyte Multilayers as Dielectric Spacers. *Angew. Chem., Int. Ed.* **2014**, *53*, 866–870.
16. Geddes, C. D.; Lakowicz, J. R. Metal-Enhanced Fluorescence. *J. Fluoresc.* **2002**, *12*, 121–129.
17. Lakowicz, J. R. Radiative Decay Engineering 5: Metal-Enhanced Fluorescence and Plasmon Emission. *Anal. Biochem.* **2005**, *337*, 171–194.
18. Li, X.; Qian, J.; Jiang, L.; He, S. Fluorescence Quenching of Quantum Dots by Gold Nanorods and Its Application to DNA Detection. *Appl. Phys. Lett.* **2009**, *94*, 063111.
19. Horimoto, N. N.; Imura, K.; Okamoto, H. Dye Fluorescence Enhancement and Quenching by Gold Nanoparticles: Direct Near-Field Microscopic Observation of Shape Dependence. *Chem. Phys. Lett.* **2008**, *467*, 105–109.
20. Schneider, G.; Decher, G. Distance-Dependent Fluorescence Quenching on Gold Nanoparticles Ensheathed with Layer-by-Layer Assembled Polyelectrolytes. *Nano Lett.* **2006**, *6*, 530–536.
21. Reineck, P.; Gómez, D.; Ng, S. H.; Karg, M.; Bell, T.; Mulvaney, P.; Bach, U. Distance and Wavelength Dependent Quenching of Molecular Fluorescence by Au@SiO<sub>2</sub> Core–Shell Nanoparticles. *ACS Nano* **2013**, *8*, 6636–6648.
22. Cheng, D.; Xu, Q.-H. Separation Distance Dependent Fluorescence Enhancement of Fluorescein Isothiocyanate by Silver Nanoparticles. *Chem. Commun.* **2007**, *43*, 248–250.
23. Kümmerlen, J.; Leitner, A.; Brunner, H.; Ausseneegg, F. R.; Wokaun, A. Enhanced Dye Fluorescence over Silver Island Films: Analysis of the Distance Dependence. *Mol. Phys.* **1993**, *8*, 1031–1046.
24. Tam, F.; Goodrich, G. P.; Johnson, B. R.; Halas, N. J. Plasmonic Enhancement of Molecular Fluorescence. *Nano Lett.* **2007**, *7*, 496–501.
25. Geddes, C. D. *Metal-Enhanced Fluorescence*, 1st ed.; John Wiley & Sons, Inc.: Hoboken, NJ, 2010.

26. Arunkumar, E.; Fu, N.; Smith, B. D. Squaraine-Derived Rotaxanes: Highly Stable, Fluorescent Near-IR Dyes. *Chem.—Eur. J.* **2006**, *12*, 4684–4690.
27. Lakowicz, J. R. Plasmonics in Biology and Plasmon-Controlled Fluorescence. *Plasmonics* **2006**, *1*, 5–33.
28. IRDye Infrared Dyes. <http://www.licor.com/bio/products/reagents/irdye> (accessed May 7, 2013).
29. Gorelikov, I.; Matsuura, N. Single-Step Coating of Mesoporous Silica on Cetyltrimethyl Ammonium Bromide-Capped Nanoparticles. *Nano Lett.* **2008**, *8*, 369–373.
30. Stöber, W.; Fink, A.; Bohn, E. Controlled Growth of Mono-disperse Silica Spheres in the Micron Size Range. *J. Colloid Interface Sci.* **1968**, *26*, 62–69.
31. Holb, H. C.; Finn, M. G.; Sharpless, K. B. Click Chemistry: Diverse Chemical Function from a Few Good Reactions. *Angew. Chem., Int. Ed.* **2001**, *40*, 2004–2021.
32. Agard, N. J.; Prescher, J. A.; Bertozzi, C. R. A Strain-Promoted [3 + 2] Azide-Alkyne Cycloaddition for Covalent Modification of Biomolecules in Living Systems. *J. Am. Chem. Soc.* **2004**, *126*, 15046–15047.
33. Sau, T. K.; Murphy, C. J. Room Temperature, High-Yield Synthesis of Multiple Shapes of Gold Nanoparticles in Aqueous Solution. *J. Am. Chem. Soc.* **2004**, *126*, 8648–8649.
34. DeVetter, B. M.; Bhargava, R.; Murphy, C. J. Computational Study of the Surface-Enhanced Raman Scattering from Silica-Coated Silver Nanowires. *Photochem. Photobiol.* **2014**, *90*, 415–418.
35. Rodríguez-Fernández, J.; Pastoriza-Santos, I.; Pérez-Juste, J.; García de Abajo, F. J.; Liz-Marzán, L. M. The Effect of Silica Coating on the Optical Response of Sub-micrometer Gold Spheres. *J. Phys. Chem. C* **2007**, *111*, 13361–13366.
36. Nooney, R. I.; Dhanasekaran, T.; Chen, Y.; Josephs, R.; Ostafin, A. E. Self-Assembly of Mesoporous Nanoscale Silica/Gold Composites. *Langmuir* **2003**, *19*, 7628–7637.
37. Zhan, Q.; Qian, J.; Li, X.; He, S. A Study of Mesoporous Silica-Encapsulated Gold Nanorods as Enhanced Light Scattering Probes for Cancer Cell Imaging. *Nanotechnology* **2010**, *21*, 055704.
38. Cuitentes, A.; Bernal, J. L.; Diez-Masa, J. C. Determination of the Critical Micelle Concentration Values Using Capillary Electrophoresis Instrumentation. *Anal. Chem.* **1997**, *69*, 4271–4274.
39. Sun, S.; Wu, P. Mechanistic Insights into Cu(II)-Catalyzed Azide-Alkyne “Click” Cycloaddition Monitored by Real Time Infrared Spectroscopy. *J. Phys. Chem. A* **2010**, *114*, 8331–8336.
40. Kar, M.; Bharmana, M.; Das, A.; Panneri, S.; Gupta, S. S. Synthesis and Characterization of Poly-L-lysine Grafted SBA-15 Using NCA Polymerization and Click Chemistry. *J. Mater. Chem.* **2011**, *21*, 6690–6697.
41. Kühn, S.; Häkanson, U.; Rogobete, L.; Sandoghdar, V. Enhancement of Single-Molecule Fluorescence Using a Gold Nanoparticle as an Optical Nanoantenna. *Phys. Rev. Lett.* **2006**, *97*, 017402.
42. Dvoynenko, M. M.; Wang, J.-K. Revisiting Coupling between a Single Molecule and Surface Plasmons. *Opt. Lett.* **2013**, *5*, 760–762.
43. Nerkararyan, K. V.; Bozhevolnyi, S. I. Relaxation Dynamics of a Quantum Emitter Resonantly Coupled to a Metal Nanoparticle. *Opt. Lett.* **2014**, *6*, 1617–1620.
44. Barthes, J.; Bouhelier, A.; Dereux, A.; des Francs, G. C. Coupling of a Dipolar Emitter into One-Dimensional Surface Plasmon. *Sci. Rep.* **2013**, *3*, 2734.
45. Akimov, A. V.; Mukherjee, A.; Yu, C. L.; Chang, D. E.; Zibrov, A. S.; Hemmer, P. R.; Park, H.; Lukin, M. D. Generation of Single Optical Plasmons in Metallic Nanowires Coupled to Quantum Dots. *Nature* **2007**, *450*, 402–406.
46. Lakowicz, J. R. *Principles of Fluorescence Spectroscopy*, 2nd ed.; Kluwer Academic/Plenum Publishers: New York, 1999; pp 51–101.
47. Anger, P.; Bharadwaj, P.; Novotny, L. Enhancement and Quenching of Single-Molecule Fluorescence. *Phys. Rev. Lett.* **2006**, *96*, 113002.
48. Lakowicz, J. R. Radiative Decay Engineering: Biophysical and Biomedical Applications. *Anal. Biochem.* **2001**, *298*, 1–24.
49. Guzatov, D. V.; Klimov, V. V. Radiative Decay Engineering by Triaxial Nanoellipsoids. *Chem. Phys. Lett.* **2005**, *412*, 341–346.
50. Moroz, A. Non-radiative Decay of a Dipole Emitter Close to a Metallic Nanoparticle: Importance of Higher-Order Multipole Contributions. *Opt. Commun.* **2010**, *283*, 2277–2287.
51. Carminati, R.; Greffet, J. J.; Henkel, C.; Vigoureux, J. M. Radiative and Non-radiative Decay of a Single Molecule Close to a Metallic Nanoparticle. *Opt. Commun.* **2006**, *261*, 368–375.
52. Novotny, L.; Hecht, B. *Principles of Nano-Optics*, 2nd ed.; Cambridge University Press: Cambridge, UK, 2012.
53. He, G. S.; Zhu, J.; Yong, K.-T.; Baev, A.; Cai, H.-Z.; Hu, R.; Cui, Y.; Zhang, X.-H.; Prasad, P. N. Scattering and Absorption Cross-Section Spectral Measurements of Gold Nanorods in Water. *J. Phys. Chem. C* **2010**, *114*, 2853–2860.
54. Ming, T.; Chen, H. J.; Jiang, R. B.; Li, Q.; Wang, J. F. Plasmon-Controlled Fluorescence: Beyond the Intensity Enhancement. *J. Phys. Chem. Lett.* **2012**, *3*, 191–202.
55. Yang, J.; Shen, D.; Zhou, L.; Li, W.; Fan, J.; El-Toni, A. M.; Zhang, W.; Zhang, F.; Zhao, D. Mesoporous Silica-Coated Plasmonic Nanostructures for Surface-Enhanced Raman Scattering Detection and Photothermal Therapy. *Adv. Healthcare Mater.* **2014**, DOI: 10.1002/adhm.201400053.
56. Zhou, S.; Sha, H.; Liu, B.; Du, X. Integration of Simultaneous and Cascade Release of Two Drugs into Smart Single Nanovehicles Based on DNA-Gated Mesoporous Silica Nanoparticles. *Chem. Sci.* **2014**, DOI: 10.1039/C4SC01195C.
57. Wu, P.; Brand, L. Resonance Energy Transfer: Methods and Applications. *Anal. Biochem.* **1994**, *218*, 1–13.
58. Zhao, L.; Ming, T.; Shao, L.; Chen, H. J.; Wang, J. F. Plasmon-Controlled Förster Resonance Energy Transfer. *J. Phys. Chem. C* **2012**, *116*, 8287–8296.
59. Ayala-Orozco, C.; Liu, J. G.; Knight, M. W.; Wang, Y.; Day, J. K.; Nordlander, P.; Halas, N. J. Fluorescence Enhancement of Molecules Inside a Gold Nanomatrixyoshka. *Nano Lett.* **2014**, *14*, 2926–2933.
60. Vukovic, S.; Corni, S.; Mennucci, B. Fluorescence Enhancement of Chromophores Close to Metal Nanoparticles. Optimal Setup Revealed by the Polarizable Continuum Model. *J. Phys. Chem. B* **2009**, *113*, 121–133.
61. Khatua, S.; Paulo, P. M. R.; Yuan, H.; Gupta, A.; Zijlstra, P.; Orrit, M. Resonant Plasmonic Enhancement of Single-Molecule Fluorescence by Individual Gold Nanorods. *ACS Nano* **2014**, *8*, 4440–4449.
62. Orendorff, C. J.; Murphy, C. J. Quantitation of Metal Content in the Silver-Assisted Growth of Gold Nanorods. *J. Phys. Chem. B* **2006**, *110*, 3990–3994.